Investigation of Mn Promotion on HKUST-1 Metal-Organic Frameworks for Low-Temperature Selective Catalytic Reduction of NO with NH 3

Katarzyna Świrk, Gérard Delahay, Abdelali Zaki, Karim Adil, Amandine Cadiau

▶ **To cite this version:**

Katarzyna Świrk, Gérard Delahay, Abdelali Zaki, Karim Adil, Amandine Cadiau. Investigation of Mn Promotion on HKUST-1 Metal-Organic Frameworks for Low-Temperature Selective Catalytic Reduction of NO with NH 3. ChemCatChem, 2021, 13 (18), pp.4029-4037. 10.1002/cctc.202100431 . hal-03351240

HAL Id: hal-03351240
https://hal.science/hal-03351240

Submitted on 22 Sep 2021

HAL is a multi-disciplinary open access archive for the deposit and dissemination of scientific research documents, whether they are published or not. The documents may come from teaching and research institutions in France or abroad, or from public or private research centers.

L'archive ouverte pluridisciplinaire **HAL**, est destinée au dépôt et à la diffusion de documents scientifiques de niveau recherche, publiés ou non, émanant des établissements d'enseignement et de recherche français ou étrangers, des laboratoires publics ou privés.

Investigation of Mn promotion on HKUST-1 metal-organic frameworks for low-temperature selective catalytic reduction of NO with NH_3

Katarzyna Świrk*, Gérard Delahay, Abdelali Zaki, Karim Adil, Amandine Cadiau*[a]

[a] Dr. K. Świrk, Dr. G. Delahay, Dr. A. Zaki, Dr. K. Adil, Dr. A. Cadiau
ICGM, Univ. Montpellier, CNRS, ENSCM, Montpellier, France
E-mail: K. Świrk katarzyna.swirk@ntnu.no (present address: Norwegian University of Science and Technology (NTNU), Department of Chemical Engineering, 7491 Trondheim, Norway); A.Cadiau amandine.cadiau@yahoo.fr

Supporting information for this article is given via a link at the end of the document.

Abstract: A series of HKUST-1 supported catalysts (also known as Cu-BTC, or MOF-199 [copper(II)-benzene-1,3,5-tricarboxylate]) modified with different loadings of managanese were synthesized and characterized by powder X-ray diffraction, scanning electron microscopy/energy dispersive spectroscopy, nitrogen sorption, thermogravimetric analysis, and temperature-programmed desorption with NH_3. The structural and textural properties of the solids compared to the reference support are preserved as much as possible when the manganese content is not higher than 5 wt.%. This makes it possible to obtain effective catalysts at low temperatures (<200°C) in the selective catalytic reduction of NO with NH_3, since high specific surface area is well-retained. Higher efficiency is obtained with the catalyst containing 3.75 wt.% of manganese which exhibits NO conversion of 68% at Weight Hourly Space Velocity (WHSV) of 96,000 ml/h·g. This performance in NO reduction is recognized to be one of the best in the series of HKUST-1-Mnx catalysts. Nevertheless, their narrow temperature window for the working reaction and sensitivity to the presence of water vapor and sulfur dioxide remain a drawback.

Introduction

Nitrogen oxides (NOx = NO and NO_2) are harmful gases formed during combustion of fossil fuels in the stationary energy sources, or in the engines of gasoline and diesel cars. NOx emissions are essential contributors to current air pollution problems, such as greenhouse effect, photochemical smog, or acid rains. In addition, nitrogen oxides pose a serious risk to human health, i.e. numerous respiratory problems. Hence, the removal of NOx is of paramount importance.[1] One of the well-established technologies for reduction of NOx emissions abatement in stationary sources is selective catalytic reduction with NH_3 (NH_3-SCR). The conventional catalyst used for SCR is V_2O_5-WO_3(MoO_3)/TiO_2 deposited on a monolith. The operating temperature window is from 300 to 400ºC, prompting a necessity of application of the catalyst on a “high-dust” position, where temperature is sufficient for its operation. Unfortunately, in this configuration the catalyst may undergo fast deactivation due to presence of dust, SO_2 and/or alkaline metals. Thus, more adequate would be locating a catalyst in a “tail-end” position where the deactivation effect can be weakened. The latter requires a catalytic material that works effectively in a low-temperature window (under 250ºC).

The development of catalysts has progressed rapidly over the past twenty-five years. Copper materials become one of the most interesting catalysts as both copper ions, Cu(I) and/or Cu(II), play important role in NH_3-SCR.[2,3] Metal oxides, mixed metal oxides, and zeolites were found very promising in NH_3-SCR. Unfortunately, in most cases, they do not reveal high activity below 250ºC.[4,5] This does not solve the problem of low-temperature operation demand. Lately, metal-organic frameworks (MOFs) attracted much interest mostly due to their multifunctional properties.[6–10] Their enhanced textural features (high S_{BET} and tunable pore size), very good adsorption properties, and proper acidity make them good candidates for catalysis field. Still, metal-organic frameworks are scarcely reported for NH_3-SCR, and only several reports may be found in this research area.[11–21] HKUST-1 is one of the most popular MOFs used for adsorption, air purification, and gas separation of molecules such as, for example, NH_3,[22] H_2O,[23] CO_2,[24] CH_4, or H_2.[25] HKUST-1 has been reported for the first time in 1999.[26] The material is also known as Cu-BTC, MOF-199, and commercially available under the name of Basolite® C300. Its octahedral structure is formed by the central cation of Cu^{2+} and benzene-1,3,5-tricarboxylate (BTC) as the linker.

To the best of our knowledge, only five reports can be found on selective catalytic reduction of NO with NH_3 over HKUST-1 catalysts.[18–21,27] Testing procedure in the above-mentioned studies mainly assumes a pre-treatment at different temperatures ranged from 150

to 260ºC, equivalent amount of NO and NH_3 (1000 ppm or 500 ppm), and oxygen content of 2 or 5 vol.%. [18–21] Higher temperature than ca. 280ºC results in total decomposition of Cu-BTC structure, consequently leading to CuO formation. Furthermore, the authors reported NO conversion results without presenting the evolution of NH_3.[18–21] In our recently published article we showed the importance of operation conditions, pointing to the negative effect of the elevated temperatures on the catalysts' structure.[27] In other words, above 185ºC we indicated a partial decomposition of metal-organic frameworks recognized by presence of the mass signals arising from carbon dioxide and carbon. The influence of metal promotion (V, Nb and Mn) in HKUST-1 for NH_3-SCR was also examined. The most promising results were found for Mn (2.5 wt.%) containing HKUST-1, giving 80% and 100%, respectively for NO and NH_3 conversions, assuming Weight Hourly Space Velocity (WHSV) of 80,000 ml/g·h. The operation temperature of the catalytic process, as well as the temperature of pre-treatment was 185ºC. In the existing literature, many examples can be found on the promoting effect of manganese in the NH_3-SCR process due to labile surface oxygen species that can complete the catalytic cycle, consequently improving activity at low temperatures. Mn-containing catalysts demonstrate high activity and selectivity in low-temperature NH_3-SCR due to the unique redox property of MnOx species.[28–32]

Yao et al.[18] described fabrication of HKUST-1 with Mn contents from 2.8 to 3.4 at.%, presuming synthesis of Cu-BTC powder and its dispersion in the ethanol solutions containing different loadings of Mn. The samples were transferred into stainless steel autoclave at 90ºC for 24h, and subsequently filtered, washed with ethanol and distilled water. The samples were finally dried under vacuum at 100ºC overnight. On the contrary, our study characterizes simplicity of the sample preparation in which a facile incipient wetness impregnation method with Mn solutions ultrasonically dispersed in water and subsequent drying at 70ºC overnight were applied.

Herein, we present the catalytic performance of HKUST-1 impregnated with different loadings of manganese (2.5, 3.75, 5.0, 7.5 and 10 wt.%) in selective catalytic reduction of NO with NH_3. The novelty of our work lays in (i) the preparation method of the HKUST-1-Mn catalysts, (ii) examination of Mn loadings ranged from 2.5 to 10 wt.%, (iii) the lower operating temperature, and (iv) higher content of oxygen (8 vol.%) in the reaction feed compared to the previously reported studies on MOFs for SCR. Furthermore, in this work the influence of SO_2 in NH_3-SCR over HKUST-1 (Cu-BTC) catalysts is examined for the first time.

Results and Discussion

The structural and textural features were confirmed by PXRD, SEM/EDS and N_2 sorption characterization methods.

Figs. 1A,B present PXRD patterns of as-synthesized materials. The commercial Basolite® C300 (here as HKUST-1) revealed a face-centered cubic crystal lattice of the *Fm3m* space group with characteristic reflections of (200), (220), (222), (400), (333) and (440) planes at 2θ = 6.7°, 9.5°, 11.7°, 13.5°, 17.4°, 19.3°, respectively.[21,33] After modification with different loadings of Mn, the reflections were preserved, although their intensities became significantly lower when the metal loading was higher than 5.0 wt.%. Figs. 1A,B show the XRD patterns multiplied by 10 and 20, respectively for the samples with the presumed Mn content of 7.5 and 10 wt.%. For these catalysts a lack of (220) plane was observed, implying a loss of crystallinity and the presence of defects in the crystal lattice of HKUST-1.[20,34] For all catalysts, a noticeable shift of PXRD reflections, in respect to HKUST-1, implies an existence of new cation or formation of new bonding (Fig. 1A).[35,36] This slight disturbance of the lattice could be also linked with lower intensities. No separate phase of manganese species was detected for the Mn-modified samples (Fig. 1B), suggesting their amorphous character and/or well-dispersion over the support.[37,38] More exposed active sites account for the better catalytic performance in NH_3-SCR.

Fig. 2 shows micrographs of Mn-containing samples. The well-defined octahedral crystals with sharp edges are maintained for the HKUST-1-Mn2.5, HKUST-1-Mn3.75, and HKUST-1-Mn5.0 catalysts, being very similar to the commercial product presented in our previous study.[27] The minor cracks on crystals can be observed in SEM micrographs, similarly to those reported previously.[18]

The modification with 7.5 and 10 wt.% resulted in a partial destruction of the MOF crystals, hardly revealing the octahedron structure with unsharpened edges. This is in line with PXRD results, in which a significant loss of crystallinity was registered. Furthermore, with the increasing loading of manganese the outer surface of the catalysts became rougher as a consequence of deposition of the metal species. For all samples, the magnification (x 2.0 μm) revealed formation of evenly distributed layers. Similar morphologies were found for Mn-containing samples in the study of Bastos et al.[39], and ascribed to the different phases of MnOx species. In our study, one can note that the porosity of the surface decreased with the increasing loading of metal. The HKUST-1-Mn7.5 and HKUST-1-Mn10 catalysts, showed more compact morphology with less pores which is in contrast to the materials modified with Mn ranging from 2.5 to 5.0 wt.%.

EDS analysis was employed to examine the elemental composition of external surface of the studied catalysts (Table 1). The atomic concentrations of C, Cu and Mn were calculated as the average of the five spots captured for each sample. The content of oxygen was excluded. The surface concentration of carbon and copper was in the range of 90.7 – 79.76 at.% and 9.3 – 8.65 at.%, respectively. Both decreased with the increasing content of Mn (1.59 – 11.6 at.%). For the HKUST-1-Mn2.5, -Mn3.75, and -Mn5.0 catalysts, very similar amount of Mn has been detected (ranging from 1.59 – 2.43 at.%), which implies that some Mn atoms were located in the pores.[40] The calculated C/Cu atomic ratio was 9.1 – 10.0, in good agreement with those observed in other literature studies.[18,41]

Mn/Cu atomic ratio ranged from 0.16 to 1.34, additionally highlighting a difference with the other study on $Mn@Cu_2(BTC)_2$ in which lower Mn loading was examined.[18] The distribution of metal ions was analyzed by EDS elemental mapping. The mapping results are presented in Fig. S1, showing that Mn element is distributed in the area of crystalline particles. This supports the existence of uniformly dispersed manganese metals in the microcrystalline sample. The elemental maps obtained for HKUST-1-Mn3.75 and HKUST-1-Mn5.0 catalysts showed that less Mn can be found on the outer surface compared to the other Mn-modified catalysts.

The isotherms and pore size distribution analyzed by N_2 sorption technique are presented in Fig. 2A,B. The adsorption/ desorption isotherms of HKUST-1 catalyst is of type I, typical for microporous material.[42] The specific surface area (SSA) is 1709 m^2/g, in good agreement with the material specification stated by the provider. The measured S_{BET} values were in range of 1315 to 451 m^2/g, gradually decreasing with the increasing Mn loading (Table 2). Although the promotion with Mn species was not favorable in terms of specific surface area, the measured SSA still showed a high value, particularly after the modification with 2.5, 3.75 and 5.0 wt.%. Furthermore, following the modification with different contents of Mn, the isotherms became a combination of type I and IV with apparent hysteresis loops, indicating the presence of both micropores and mesopores.[42,43] The volume of micropores decreased at the expense of the volume of mesopores in the Mn-containing materials (Table 1).

The formation of mesopores can be considered valuable for providing the bulkier substances (NH_3, NO) with the access to the active sites of MOF.[19,42] The BJH pore size distribution (PSD) of Mn-modified materials is presented in Fig. 2B. The pore size distribution was found to be typical for HKUST-1, revealing a pore size distributed along with the range of 37 - 44 Å.[44] Upon modification with Mn, the mesopores are formed with diameter becoming wider with the increasing Mn loading. This agrees well with the measured V_{mes}. The Mn2.5, 3.75 and 5.0

catalysts showed pore size distributed between 44 - 92 Å, whereas higher loading than 5.0 wt.% resulted in formation of wider mesopores (44 - 118 Å). The average pore diameters are listed in Table 2, varying from 34 to 74 Å. As SEM/EDS analysis confirmed, the metals were present on the outer surface of the studied samples and the magnified images revealed the presence of species with laminar structure. The decoration of the surface by metal precursors is also confirmed by a decrease in SSA and V_{mic} calculated for the modified catalysts. Some cations are also present inside the pores of HKUST-1, as supported by formation of many peaks with pore size lower than the one determined for the parent material. This is in good agreement with elemental surface analysis carried out by EDS in which atomic surface concentration was significantly low for the samples with the assumed loading up to 5 wt.%. The metal content of 7.5 and 10 wt.% resulted in the creation of wider pores in the range of ca. 30 - 44 Å. No pores smaller than those observed for the parent material were registered in HKUST-1-Mn7.5 and HKUST-1-Mn10.0 catalysts.

According to Gallagher et al.[45], a decomposition of manganese (II) nitrate hydrate in inert atmosphere, also performed in our study, involves H_2O and NO_2 removal in the temperature range from 178 to 260°C. The resulting residue is $MnONO_3$ or MnO_2. The latter is stable till 500°C.[45] Getzschmann et al.[46] described three different types of pores present in the HKUST-1: (i) small pores with diameter of ca. 5 Å, calculated as twice the distance between the center of the pore and the center of the benzene ring minus twice the van der Waals radius of a carbon atom of 1.7 Å; (ii) larger pores with diameter of ca. 11 Å, representing the octahedral holes of an fcc structure;

(iii) the largest pores of ca. 13.5 Å, calculated as twice the distance between the center of the pore and the copper atom minus twice the van der Waals radius of copper (1.4 Å). Since the ionic radii of Mn^{3+} (0.645 Å) and Mn^{4+} (0.53 Å) are smaller than cavities of HKUST-1, it seems plausible that manganese ions can enter into pores and interact with constrictive elements of the MOF.[47] Furthermore, the existence of Mn^{3+} and Mn^{4+} has been also confirmed for $Mn@Cu_2(BTC)_2$ catalysts tested in NH_3-SCR in the study of Yao et al.[18]

Thermogravimetric analysis (TGA) was employed to study thermal stability of the studied catalysts. The measurements were carried out in air to determine the temperature of decomposition of each material. The catalytic performance of the calcined HKUST-1-Mn is not the scope of this research. Fig. S2 depicts TGA curves where a similar trend was found consisting of three main mass losses. The first weight loss between 40 to 120ºC is assigned to

removal of physically adsorbed water molecules. Second mass loss occurred between ca. 120 and 270ºC, and can be ascribed to slow removal of residual water molecules together with the solvent which is physically adsorbed in internal pores.[35] At temperature of ca. 200ºC, the structure starts to release the water that is chemically bonded. Above ca. 270ºC, the mass loss rate rapidly increased which can be linked to the structure collapse caused by the decomposition of the BTC organic linkers. The remaining weight in HKUST-1 catalysts is only ca. 32% with residue in the form of CuO and $CuMn_2O_4$.[27] Upon modification with manganese thermal stability of the resulting materials did not change.

Ammonia temperature-programmed desorption (NH_3-TPD) was performed to evaluate acidic properties of Mn-promoted MOFs. The ammonia desorption profiles are shown in Fig. S3. It has to be stressed, that in order to avoid a possible interference of TCD with water, the samples were pretreated till 240ºC.[27] With increasing Mn loading the acidity of the materials increased, as confirmed by the obtained desorption profiles. The registered curves did not reveal any significant peak, which is in good agreement with the previously published reports on HKUST-1.[27,48] As a whole, the modification with Mn increased acidity of the catalysts, contributing to the enhanced catalytic performance in the NH_3-SCR process. The loadings of 7.5 wt.% and 10.0 wt.% showed the same curves of NH_3 desorption, indicating that higher loading than the former does not have significant influence on the acidic properties.

Selective catalytic reduction of NO with NH_3 was investigated on Mn-promoted MOFs and compared to the unmodified HKUST-1 using [NO] = 1000 ppm, [NH_3] = 1000 ppm, [O_2] = 8 vol.% in the absence of water. According to the activity results, the manganese content rather than the specific surface area plays more important role. The following activity ranking can be observed: Mn3.75 > Mn2.5 > Mn5.0 > Mn7.5 > Mn10.0 > support. In the existing literature, manganese was found to promote zeolite-based catalysts in SCR of NOx with NH_3, e.g. in Cu-SAPO-34 catalysts or Cu-SSZ-13.[40,53,54] The beneficial effect of manganese on Cu/SAPO and Mn@$Cu_2(BTC)_2$ catalysts has been attributed to the generation of Mn^{3+} and Mn^{4+} species, or the presence of MnO_4, whereas the impregnated MnO_x species markedly improved the redox ability of Cu-SSZ-13 catalysts. Only a few studies can be found on NH_3-SCR over Mn-MOF's catalysts. Table 3 presents the most relevant literature reports regarding this matter. The catalytic results consider the NO and NH_3 conversions (X_{NO} and X_{NH3}, respectively) reported at temperature of 185°C. One can note that only three types of HKUST-1/Cu-BTC modified with Mn were studied for SCR of NO with NH_3. Among MIL-100, MOF-74, UiO-66, and HKUST-1, it appears that the one presenting the best activity is Mn-MOF-74 (75% conversion of NO)[14,49–52]. The high activity was linked with the coordinatively unsaturated sites present on Mn-MOF-74.[49] However, in all above-mentioned literature reports, the actual Mn loading in the catalysts was not well described and the NH_3 conversion was never revealed. Moreover, the comparison Table S1 indicates that in our study a high GHSV leads to similar results to those described in other publications. Among the various promoters (Nb, V, and Mn), described in our previous study [27], manganese was found to be the most active in HKUST-1-Mn2.5 when tested in NH_3-SCR at WHSV=80,000 ml/g·h at 185°C (maximum NO and NH_3 conversions of 80% and 100%, respectively). To reveal the actual activity differences between HKUST-1-Mnx catalysts, in current paper the assumed WHSV is 133,600 ml/g·h. Fig 4A presents catalytic performance of the unpromoted sample which was inactive in NH_3-SCR after 1h at 185°C. The initial NH_3 conversion and its gradual decrease were a result of the adsorption phenomena at the studied temperature. The addition of Mn led to an increase of NH_3 and NO conversions. The NO conversion was increasing with the loading of Mn from 2.5 to 5 wt.%, while it decreased with 7.5 and 10 wt.% (Fig 4). The optimal loading of Mn was found to be 3.75 wt.% with the NO and NH_3 conversions of 50% and 45%, respectively. As shown in Fig. 4D-F, higher loadings, such as 5.0, 7.5 and 10 wt.% led to 37%, 21%, 16% of NO conversion, respectively. Moreover, only N_2 and H_2O were found as products which confirms high selectivity of HKUST-1-Mnx catalysts. Our results, in terms of Mn content, agree well with those reported for Cu/SAPO catalysts with 4 wt.% of Mn loading, or

Cu/SSZ13 catalysts, where the most promising catalysts have been ascribed to the Mn content of 3 and 5 wt.% (depending on the temperature).[40,53,54] Despite small activity differences between HKUST-1-Mn2.5 and HKUST-1-Mn3.75 samples, we selected the latter to examine its resistance in the presence of H_2O and SO_2 (separately).

Water vapor and sulfur dioxide are both present as impurities in the flue gas of power plants and in the exhaust gas of vehicles. The experiments were conducted at WHSV = 96,000 ml/h·g. The introduction of H_2O into the gas feed led to a decrease of both NO and NH_3 conversions. However, when the H_2O was stopped, the conversion values have been instantly recovered. The poison effect of water may come from the reversible adsorption of H_2O which is in line with the studies on zeolites catalyst, but also on MOF's, such as Mn-MOF-74. For the latter, a recovery was observed after cycle in absence/presence/ absence of water.[40,55] In our study, just before the water feeding, the NO and NH_3 conversions were 68 and 65%, respectively. Although, a rapid decrease was reported after the introduction of H_2O with conversions found at the level of 25% and 30% for NO and NH_3, respectively (Fig 5). This could be due to the −OH species that bind to the exposed metal sites and compete with the reactive gas molecules for adsorption, in the same time reducing the active site.[56] Nevertheless, the initial conversions were finely recovered and stable after 90 min time-on-stream in the absence of water.

As shown in Fig. 5, the presence of SO_2 also resulted in a decrease of NO conversion from 68 to 48%. Similar observations were presented on Mn promoted Cu-SAPO-34 catalysts but also in Mn-MOF-74.[50,53] For the HKUST-1-Mnx series, the deactivation was constant, while after switching off the SO_2 flow a small increase of conversion was registered that did not retain the previous level before SO_2 feeding. The influence of SO_2 is more significant on catalytic behavior. An interesting behavior was observed for NH_3, which conversion did not decrease in the presence of SO_2, whereas in its absence a sharp decrease was recorded. This can be the reason of acidic properties of HKUST-1-Mn3.75 which improve in contact with SO_2. Similar observation was reported for copper and iron ZrO_2 supported catalysts.[4] A deep investigation on the effect of SO_2 is planned to be conducted in the future.

Figure 6A presents PXRD patterns of the catalysts after 6h test in NH_3-SCR. The materials contained the characteristic reflections of the parent sample, indicating that the HKUST-1 retained its structure. HKUST-1-Mn3.75 that was subjected to H_2O and SO_2 also preserved its structure (Figure 6B). However, a decrease of the crystallinity was reported to contribute to the formation of some defects in the crystal lattice. Therefore, the HKUST-1-

Mn3.75 can be considered as an efficient catalyst with both good low-temperature activity in the NH_3-SCR of NO and structural tolerance to H_2O and SO_2.

Conclusion

In this work, HKUST-1 samples rapidly impregnated with different manganese loadings of 2.5, 3.75, 5.0, 7.5, and 10 wt.% were studied in the selective catalytic reduction of NO with NH_3. The structural and textural features of HKUST-1-Mnx remained to be close to the parent HKUST-1. Manganese species possibly entered into pores of the HKUST-1 when 2.5 and 5.0 wt.% content was applied. Some Mn species were present inside and outside the surface of HKUST-1 crystals, as supported by pore size distribution and microscopy studies coupled with elemental mapping. This could be assigned to the beneficial effect of promotion with manganese that resulted in the creation of new mesopores, allowing molecules to access the framework of MOF. On the other hand, the addition of higher Mn content (7.5 and 10 wt.%) led to the partial destruction of the HKUST-1 crystals and the formation of wider pores, accompanied by a significant decrease of the microporous volume.

Manganese species participated in the selective catalytic reduction with ammonia, as only after promotion of HKUST-1 the materials became active in the studied reaction. The efficiency in NO reduction with NH_3 measured at 185°C increased with the manganese content up to 3.75 wt.% and then decreased. For HKUST-1-Mn3.75 catalyst, 68% of NO conversion was reached at 185°C (WHSV=96,000 ml/h·g). This performance into the reduction of NO with NH_3 was found to be the best for this type of catalysts (HKUST-1-Mnx). However, the operating temperature is narrow and the efficiency is remarkably reduced in the presence of H_2O and SO_2. Nevertheless, these results are encouraging and our efforts are essentially continuing to improve the stability of this type of catalyst.

Experimental Section

Sample preparation. HKUST-1-Mnx (x=2.5, 3.75, 5.0, 7.5 or 10.0) catalysts were prepared by incipient wetness impregnation using manganese (II) nitrate tetrahydrate (Sigma-Aldrich). The “x” number refers to the assumed metal loading in the individual sample in wt.%. HKUST-1 powder was purchased from Sigma-Aldrich (Basolite® C300). For the aqueous solutions, ultra-pure water was used. After the impregnation step, the samples were sonicated for 20 min at

30°C, and subsequently dried overnight at 70°C. The syntheses assumed no washing steps. The samples were activated *in situ* in helium atmosphere at 185°C prior to the catalytic tests.

Characterization methods. Powder X-ray diffraction was performed on a D8 Advance Bruker diffractometer using Cu Kα radiation source with wavelength λ=1.5406 Å. The diffractograms were obtained in an angle range of 2θ = 4–50° with a 0.02° step and an accumulation time of 1 s per step. Textural properties were determined by N_2 physisorption at −196°C using a Micromeritics ASAP 2020 apparatus. Prior to the analysis, the samples were outgassed at 150°C for 6h. The Brunauer–Emmett–Teller (BET) equation was used to calculate the specific surface area, while the Barrett–Joyner–Halenda (BJH) desorption method was applied to determine the volume of mesopores. The t-plot was used for calculation of microporous volume. The morphology of as-synthesized materials was studied by a scanning electron microscope Hitachi 4800S with an acceleration voltage of 5 kV. Energy Dispersive Spectroscopy (EDS) chemical analyses (in atomic %) were carried out on a FEI Quanta 200F (15 kV) equipment. The elemental analysis was performed with the aid of AZtec software. Thermogravimetric analysis (TGA) and differential thermal analyses (DTA) were performed by a PerkinElmer STA 6000 Simultaneous Thermal Analyzer. The material was placed in a crucible and heated in a flow of air (60 ml/min) from 40°C to 900°C with a temperature rate of 5°C/min. Temperature-programmed desorption of NH_3 (NH_3-TPD) of as-synthesized catalysts was carried out in a Micromeritics AutoChem 2910 apparatus using a thermal conductivity detector (TCD). Prior to the measurement, the samples were heated from 40°C to 250°C with a heating rate 5°C/min in order to remove H_2O molecules able to affect the TCD signal. After cooling to 140°C, the samples were saturated with NH_3 at 140°C for 30 min (a mixture 7500 ppm NH_3/He, flow rate=30 ml/min), and subsequently treated in He (flow rate=30 ml/min) for 30 min for removing physiosorbed ammonia. Finally, the NH_3-TPD profiles were determined by increasing temperature from 140 to 250°C with a heating rate of 2°C/min in helium (flow rate=30 ml/min).

Catalytic experiments. Activity in the NH_3-SCR was measured in a fixed-bed glass reactor at 185°C under the following conditions: [NO] = 1000 ppm, [NH_3] = 1000 ppm, [O_2] = 8 vol.%, He as balance, total flow 167 ml/min, mass of the catalyst 0.075 g, gas pressure 1 bar (WHSV= 133,600 ml/h·g). Prior to the catalytic test, a pre-treatment was performed in He flow (30 ml/min, heating rate 2°C/min) at 185°C. The helium flow was kept for 15 min at this temperature in order to remove guest molecules. Additionally, for the best performing sample H_2O and SO_2 tolerance was examined assuming [NO] = 1000 ppm, [NH_3]= 1000 ppm, [O_2]= 8 vol.%, [H_2O] =3.5% or

[SO_2] = 100 ppm, total flow 120 ml/min, mass of the catalyst 0.075 g, gas pressure 1 bar (WHSV= 96,000 ml/h·g). The gases were analyzed by sampling on-line to a quadrupole mass gas spectrometer Pfeiffer Vacuum equipped with Faraday and SEM detectors.

Acknowledgements

The authors acknowledge the PIA for funding with the grant ANR-18-MOPGA-0009 and the Occitanie Region. Thomas Cacciaguerra (ICGM, MACS) is greatly acknowledged for the SEM/EDS analysis.

Keywords: metal-organic framework • manganese • selective catalytic reduction • ammonia • NOx removal

References

[1] R. Abid, G. Delahay, H. Tounsi, *J. Rare Earths* **2020**, *38*, 250–256.

[2] B. Pereda-Ayo, U. De La Torre, M. J. Illán-Gómez, A. Bueno-López, J. R. González-Velasco, *Appl. Catal. B Environ.* **2014**, *147*, 420–428.

[3] M. Chen, Q. Sun, G. Yang, X. Chen, Q. Zhang, Y. Zhang, X. Yang, J. Yu, *ChemCatChem* **2019**, *11*, 3865–3870.

[4] K. Świrk, Y. Wang, C. Hu, L. Li, P. Da Costa, G. Delahay, *Catalysts* **2021**, *11*, 55.

[5] D. Pietrogiacomi, D. Sannino, A. Magliano, P. Ciambelli, S. Tuti, V. Indovina, *Appl. Catal. B Environ.* **2002**, *36*, 217–230.

[6] K. Adil, Y. Belmabkhout, R. S. Pillai, A. Cadiau, P. M. Bhatt, A. H. Assen, G. Maurin, M. Eddaoudi, *Chem. Soc. Rev.* **2017**, *46*, 3402–3430.

[7] Y. Belmabkhout, Z. Zhang, K. Adil, P. M. Bhatt, A. Cadiau, V. Solovyeva, H. Xing, M. Eddaoudi, *Chem. Eng. J.* **2019**, *359*, 32–36.

[8] W. Liang, P. M. Bhatt, A. Shkurenko, K. Adil, G. Mouchaham, H. Aggarwal, A. Mallick, A. Jamal, Y. Belmabkhout, M. Eddaoudi, *Chem* **2019**, *5*, 950–963.

[9] D. X. Xue, A. Cadiau, Ł. J. Weseliński, H. Jiang, P. M. Bhatt, A. Shkurenko, L. Wojtas, C. Zhijie, Y. Belmabkhout, K. Adil, M. Eddaoudi, *Chem. Commun.* **2018**, *54*, 6404–6407.

[10] X. Wang, X. Liu, H. Rong, Y. Song, H. Wen, Q. Liu, *RSC Adv.* **2017**, *7*, 29611–29617.

[11] S. Smolders, J. Jacobsen, N. Stock, D. De Vos, *Catal. Sci. Technol.* **2020**, *10*, 337–341.

[12] X. Sun, Y. Shi, W. Zhang, C. Li, Q. Zhao, J. Gao, X. Li, *Catal. Commun.* **2018**, *114*,

104–108.

[13] S. Li, Y. Zhai, X. Wei, Z. Zhang, X. Kong, F. Tang, *ChemCatChem* **2020**, *13, 940.*

[14] W. Zhang, Y. Shi, C. Li, Q. Zhao, X. Li, *Catal. Letters* **2016**, *146*, 1956–1964.

[15] H. Jiang, J. Zhou, C. Wang, Y. Li, Y. Chen, M. Zhang, *Ind. Eng. Chem. Res.* **2017**, *56*, 3542–3550.

[16] Y. Yu, C. Chen, C. He, J. Miao, J. Chen, *ChemCatChem* **2019**, *361021*, 979–984.

[17] P. Wang, H. Zhao, H. Sun, H. Yu, S. Chen, X. Quan, *RSC Adv.* **2014**, *4*, 48912–48919.

[18] Z. Yao, D. Qu, Y. Guo, Y. Yang, H. Huang, *Adv. Mater. Sci. Eng.* **2019**, *2019*, 1–10.

[19] C. Li, Y. Shi, H. Zhang, F. Xue, *Adv. Mater. Res.* **2015**, *1118*, 133–141.

[20] C. Li, Y. Shi, H. Zhang, Q. Zhao, F. Xue, X. Li, *Integr. Ferroelectr.* **2016**, *172*, 169–179.

[21] H. Jiang, S. Wang, C. Wang, Y. Chen, M. Zhang, *Catal. Surv. from Asia* **2018**, *22*, 95–104.

[22] E. Borfecchia, S. Maurelli, D. Gianolio, E. Groppo, M. Chiesa, F. Bonino, C. Lamberti, *J. Phys. Chem. C* **2012**, *116*, 19839–19850.

[23] N. Nijem, K. Fu, H. Bluhm, S. R. Leone, M. K. Gilles, *J. Phys. Chem. C* **2015**, *119*, 24781–24788.

[24] N. Al-Janabi, P. Hill, L. Torrente-Murciano, A. Garforth, P. Gorgojo, F. Siperstein, X. Fan, *Chem. Eng. J.* **2015**, *281*, 669–677.

[25] J. Moellmer, A. Moeller, F. Dreisbach, R. Glaeser, R. Staudt, *Microporous Mesoporous Mater.* **2011**, *138*, 140–148.

[26] S. S. Y. Chui, S. M. F. Lo, J. P. H. Charmant, A. G. Orpen, I. D. Williams, *Science (80).* **1999**, *283*, 1148–1150.

[27] K. Świrk, G. Delahay, A. Zaki, K. Adil, A. Cadiau, *Catal. Today* **2021**, *submitted*.

[28] F. Gao, X. Tang, H. Yi, S. Zhao, C. Li, J. Li, Y. Shi, X. Meng, *Catalysts* **2017**, *7*, 1–32.

[29] B. Shen, X. Zhang, H. Ma, Y. Yao, T. Liu, *J. Environ. Sci. (China)* **2013**, *25*, 791–800.

[30] M. Kang, E. D. Park, J. M. Kim, J. E. Yie, *Appl. Catal. A Gen.* **2007**, *327*, 261–269.

[31] B. Thirupathi, P. G. Smirniotis, *Appl. Catal. B Environ.* **2011**, *110*, 195–206.

[32] S. Zhang, B. Zhang, B. Liu, S. Sun, *RSC Adv.* **2017**, *7*, 26226–26242.

[33] K. Lin, A. K. Adhikari, C. Ku, C. Chiang, H. Kuo, *Int. J. Hydrogen Energy* **2012**, *37*, 13865–13871.

[34] B. Liu, Y. Li, S. C. Oh, Y. Fang, H. Xi, *RSC Adv.* **2016**, *6*, 61006–61012.

[35] A. M. P. Peedikakkal, I. H. Aljundi, *ACS Omega* **2020**, *5*, 28493–28499.

[36] J. Cheng, X. Xuan, X. Yang, J. Zhou, K. Cen, *RSC Adv.* **2018**, *8*, 32296–32303.

[37] S. A. C. Carabineiro, S. S. T. Bastos, J. J. M. Órfão, M. F. R. Pereira, J. J. Delgado, J. L. Figueiredo, *Catal. Letters* **2010**, *134*, 217–227.

[38] S. S. T. Bastos, S. A. C. Carabineiro, J. J. M. Órfão, M. F. R. Pereira, J. J. Delgado, J. L. Figueiredo, *Catal. Today* **2012**, *180*, 148–154.

[39] S. S. T. Bastos, J. J. M. Órfão, M. M. A. Freitas, M. F. R. Pereira, J. L. Figueiredo, *Appl. Catal. B Environ.* **2009**, *93*, 30–37.

[40] J. Du, J. Wang, X. Shi, Y. Shan, Y. Zhang, H. He, *Catalysts* **2020**, *10*, 1–14.

[41] H. Li, J. Qin, Y. Zhang, S. Xu, J. Du, J. Tang, *RSC Adv.* **2018**, *8*, 39352–39361.

[42] L. Yu, Q. Liu, W. Dai, N. Tian, N. Ma, *Microporous Mesoporous Mater.* **2018**, *266*, 7–13.

[43] A. Chakraborty, T. K. Maji, *APL Mater.* **2014**, 124107.

[44] R. Sule, A. K. Mishra, *Appl. Sci.* **2019**, *9*, 4407–4421.

[45] P. K. Gallagher, F. Schrey, B. Prescott, *Thermochim. Acta* **1971**, *2*, 405–412.

[46] J. Getzschmann, I. Senkovska, D. Wallacher, M. Tovar, D. Fairen-Jimenez, T. Düren, J. M. Van Baten, R. Krishna, S. Kaskel, *Microporous Mesoporous Mater.* **2010**, *136*, 50–58.

[47] S. Balaji, T. Manichandran, D. Mutharasu, *Bull. Mater. Sci.* **2012**, *35*, 471–480.

[48] W. Y. Gao, K. Leng, L. Cash, M. Chrzanowski, C. A. Stackhouse, Y. Sun, S. Ma, *Chem. Commun.* **2015**, *51*, 4827–4829.

[49] H. Jiang, Q. Wang, H. Wang, Y. Chen, M. Zhang, *ACS Appl. Mater. Interfaces* **2016**, *8*, 26817−26826.

[50] S. Xie, Q. Qin, H. Liu, L. Jin, X. Wei, J. Liu, X. Liu, Y. Yao, L. Dong, B. Li, *ACS Appl. Mater. Interfaces* **2020**, *12*, 48476–48485.

[51] S. Wang, Q. Gao, X. Dong, Q. Wang, Y. Niu, Y. Chen, H. Jiang, *Catalysts* **2019**, *9*, 1–9.

[52] M. Zhang, B. Huang, H. Jiang, Y. Chen, *Front. Chem. Sci. Eng.* **2017**, *11*, 594–602.

[53] M. Zhang, H. Cao, Y. Chen, H. Jiang, *Catal. Surv. from Asia* **2019**, *23*, 245–255.

[54] C. Pang, Y. Zhuo, Q. Weng, Z. Zhu, *RSC Adv.* **2018**, *8*, 6110–6119.

[55] G. Qi, R. T. Yang, *Appl. Catal. B Environ.* **2003**, *44*, 217–225.

[56] H. Jiang, Y. Niu, Q. Wang, Y. Chen, M. Zhang, *Catal. Commun.* **2018**, *113*, 46–50.

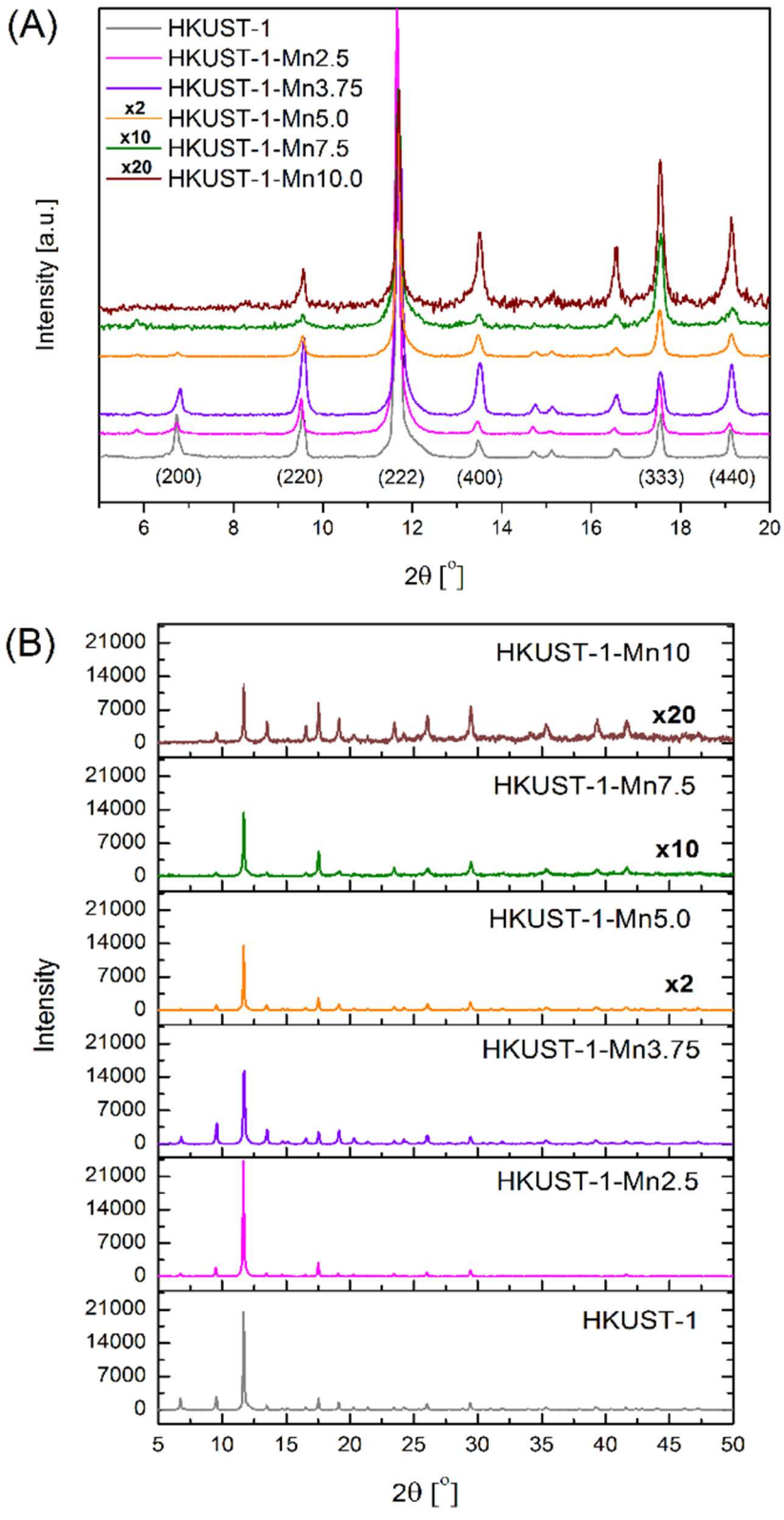

Figure 1. PXRD patterns of commercial HKUST-1 and synthesized HKUST-1-Mnx (x= 2.5, 3.75, 5.0, 7.5, 10.0) catalysts.

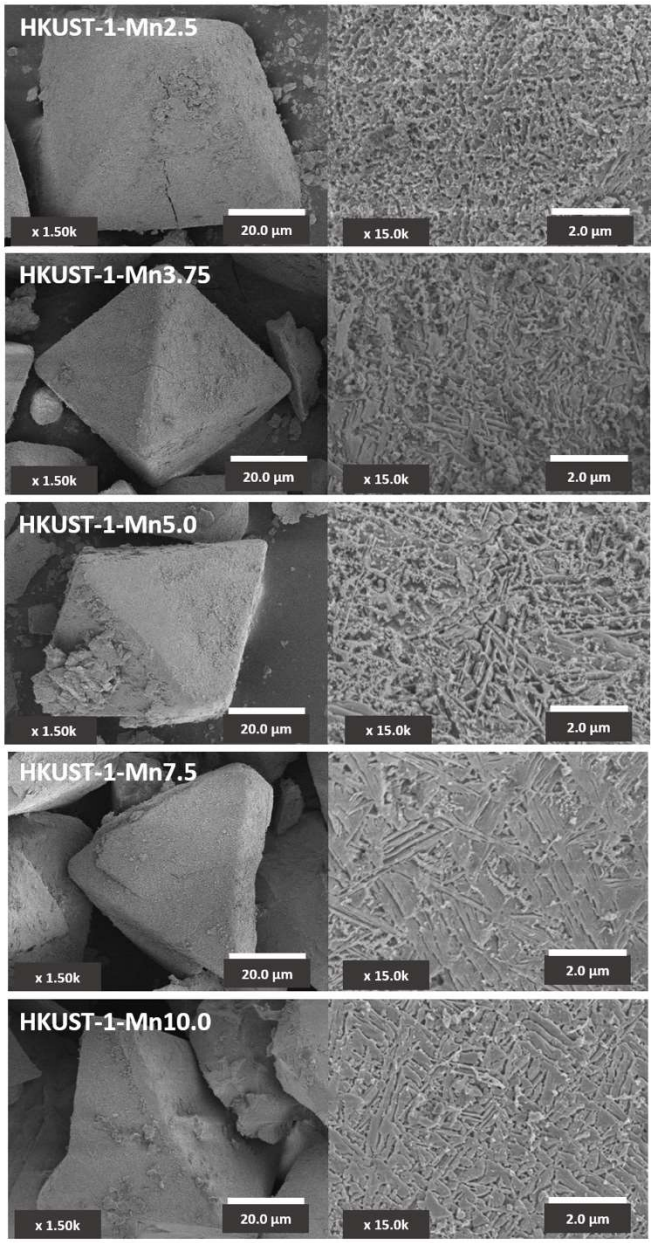

Figure 2. SEM micrographs of HKUST-1-Mnx (x= 2.5, 3.75, 5.0, 7.5, 10.0).

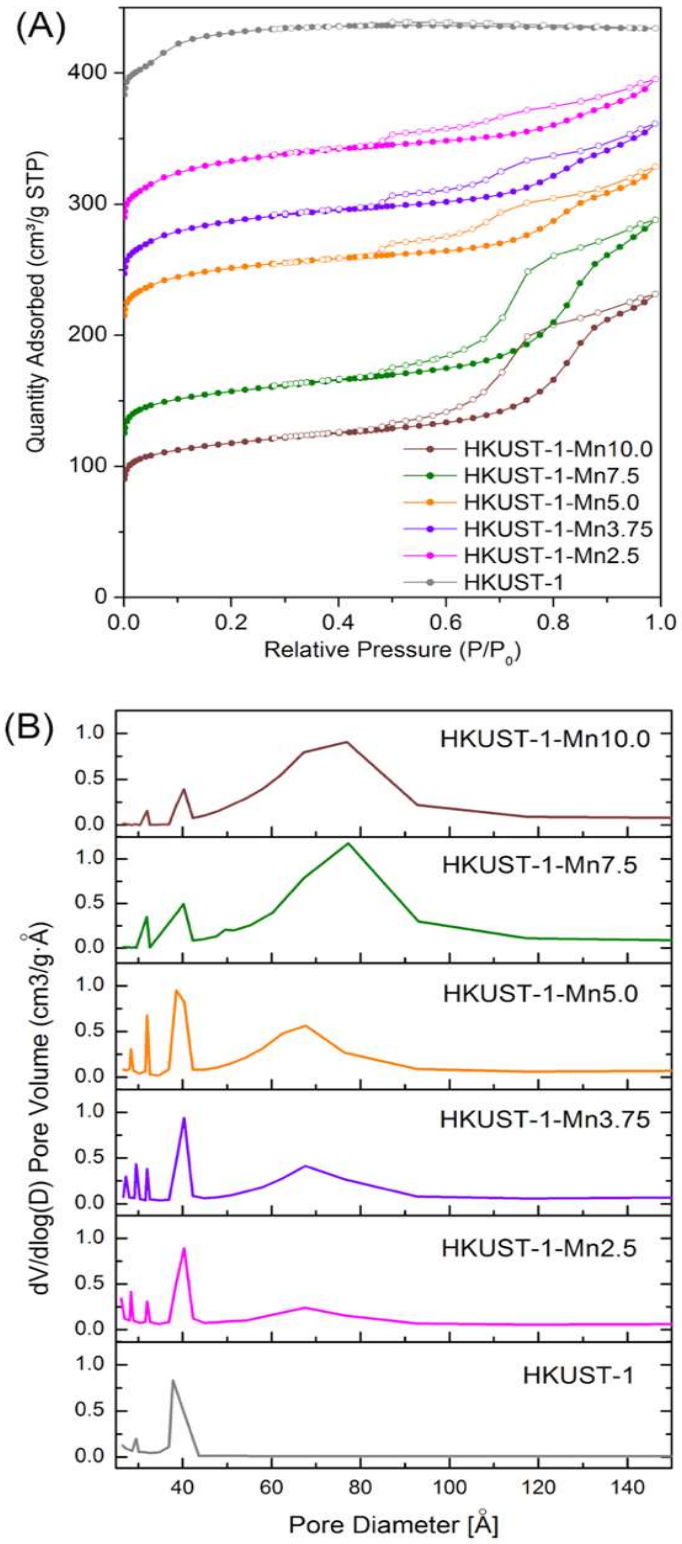

Figure 3. N_2 isotherms (A) and pore size distribution (B)

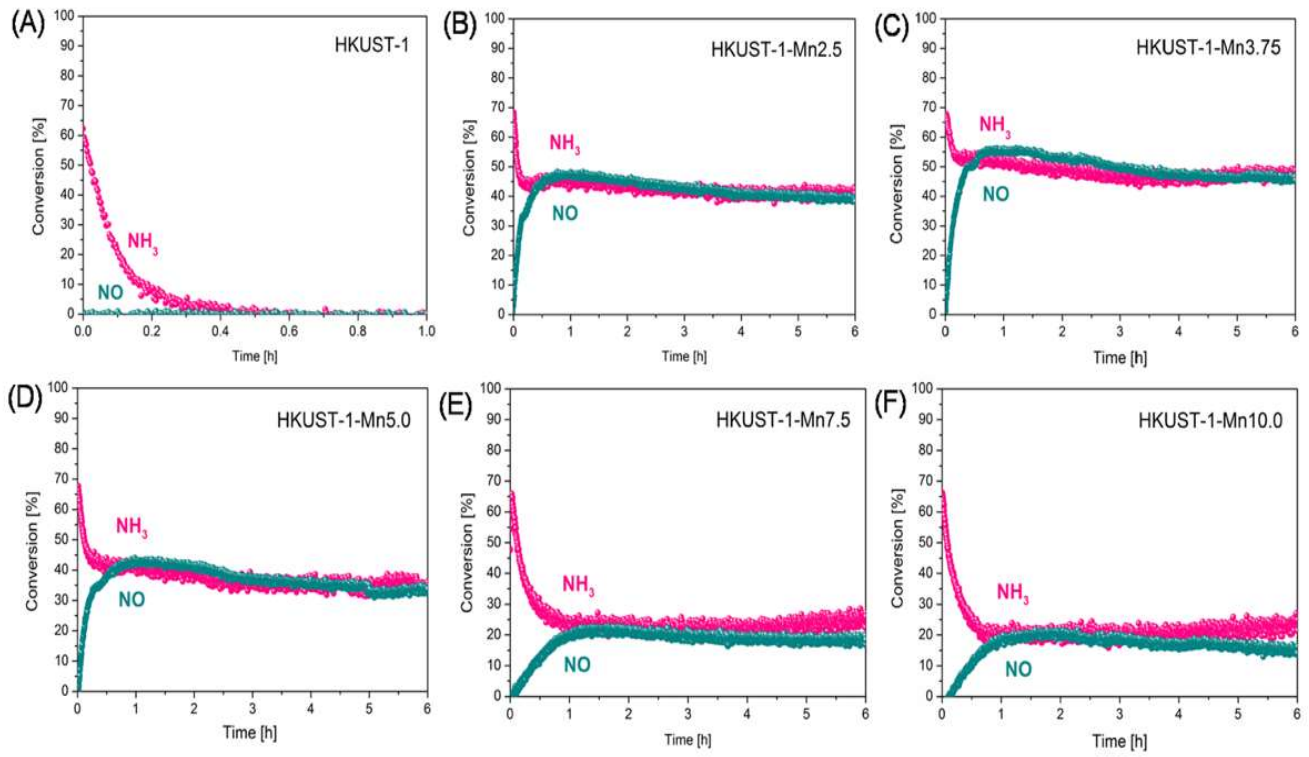

Figure 4. Catalytic performance of Mn promoted HKUST-1 catalysts at 185°C. [NO] = 1000 ppm, [NH_3] = 1000 ppm, [O_2] = 8 vol.%, He as balance, total flow 167 ml/min, mass of the catalyst 0.075 g, gas pressure 1 bar (WHSV= 133,600 ml/h·g). The catalysts were pre-treated in He flow (30 ml/min, heating rate 2°C/min) at 185°C.

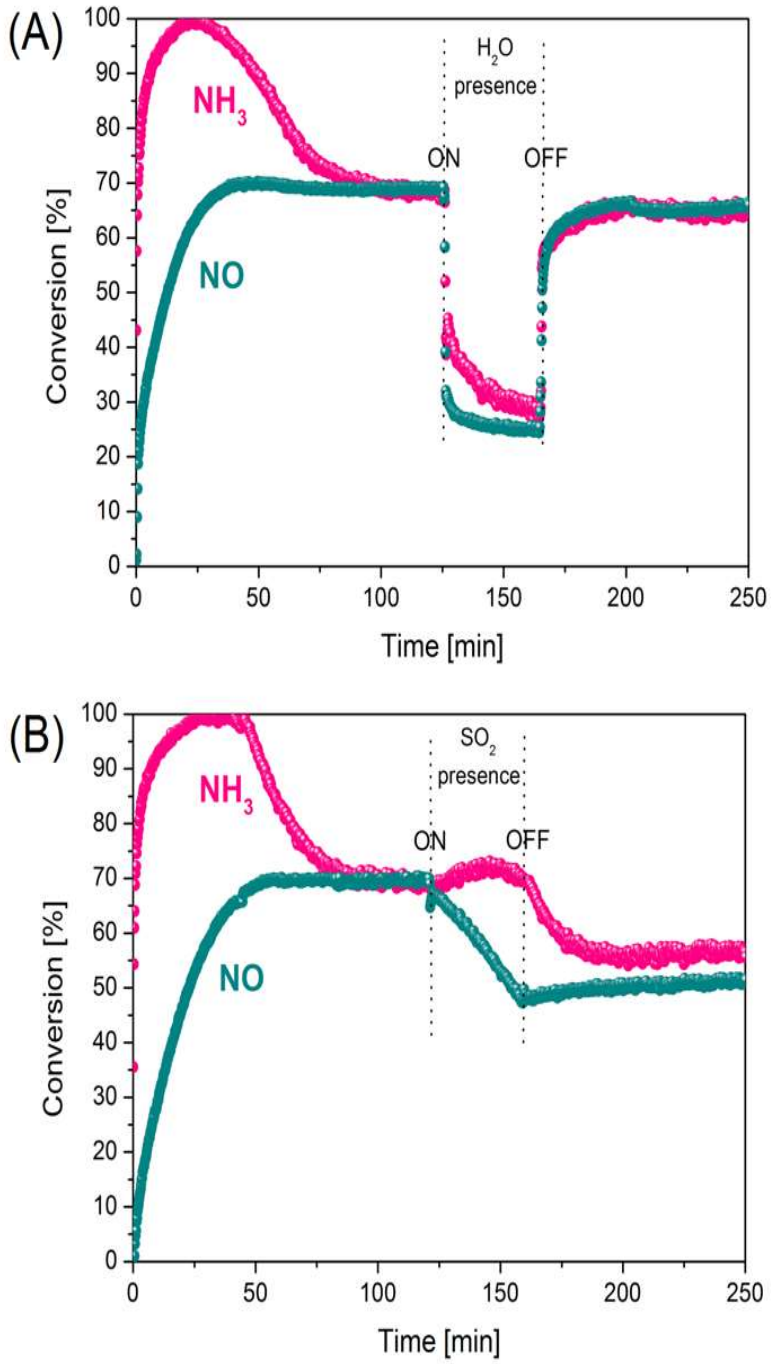

Figure 5. Catalytic performance of Mn promoted HKUST-1 catalysts. [NO] = 1000 ppm, [NH_3] = 1000 ppm, [O_2] = 8 vol.%, He as balance, total flow 120 ml/min, mass of the catalyst 0.075 g, gas pressure 1 bar (WHSV= 96,000 ml/h·g). The catalysts were pre-treated in He flow (30 ml/min, heating rate 2°C/min) at 185°C.

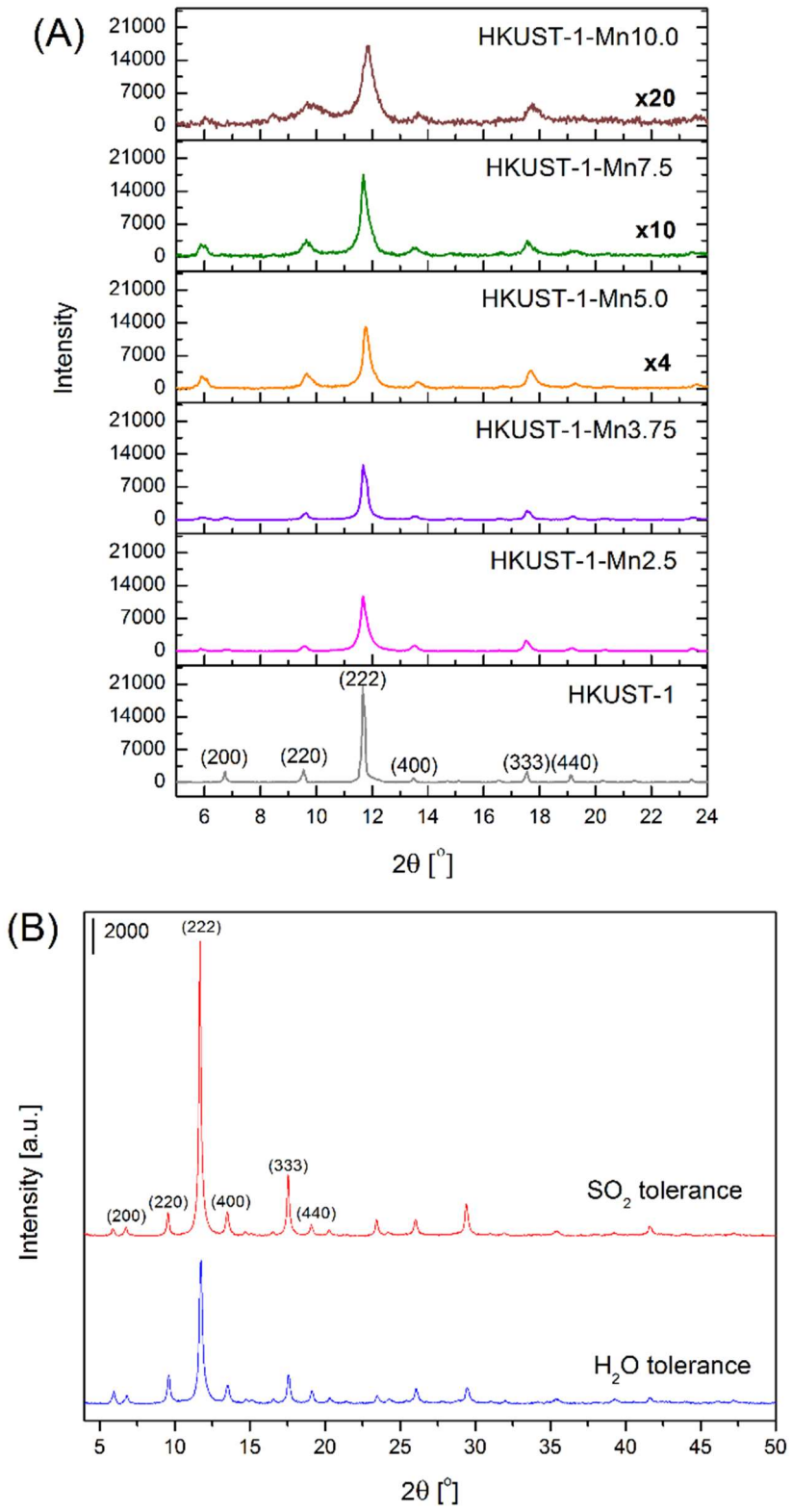

Figure 6. PXRD diffractograms of HKUST-1-Mnx catalysts after 6h test (A), and HKUST-1-Mn3.75 after NH_3-SCR tested in the presence of H_2O and SO_2 (B).

Table 1. Relative elemental composition of the studied HKUST-1-Mn catalysts (in atomic concentration [at.%]) derived from the SEM/EDS analysis. The oxygen content has been omitted.

Catalyst	C	Cu	Mn	C/Cu	Mn/Cu
HKUST-1	90.70	9.30	0	9.8	0
HKUST-1-Mn2.5	88.77	9.64	1.59	9.2	0.16
HKUST-1-Mn3.75	88.62	8.94	2.43	9.9	0.27
HKUST-1-Mn5.0	89.04	8.89	2.07	10.0	0.23
HKUST-1-Mn7.5	81.54	8.98	7.48	9.1	0.83
HKUST-1-Mn10.0	79.76	8.65	11.6	9.2	1.34

Table 2. Textural properties of Mn-promoted HKUST-1 catalysts.

Catalyst	SSA [m^2/g] [a]	V_{mic} [m^3/g] [b]	V_{mes} [m^3/g] [c]	Average pore diameter [Å] [d]
HKUST-1	1709	0.60	0.02	34
HKUST-1-Mn2.5	1315	0.44	0.13	59
HKUST-1-Mn3.75	1133	0.38	0.15	65
HKUST-1-Mn5.0	989	0.38	0.18	63
HKUST-1-Mn7.5	610	0.19	0.26	74
HKUST-1-Mn10.0	451	0.13	0.23	73

[a] calculated from the Brunauer-Emmett-Teller (BET). [b] calculated from t-plot, [c] derived from the Barrett, Joyner and Halenda (BJH) desorption method, [d] obtained from the Barrett, Joyner and Halenda (BJH) desorption method.

Table 3. Comparison of differently modified MOFs catalysts in NH_3-SCR. The X_{NO} and X_{NH3} are the values measured at 185°C.

MOF catalyst (manganese content)	NH_3-SCR	WHSV [ml/h·g]	GHSV [1/h]	X_{NO} [%]	X_{NH3} [%]	Ref.
Mn-MOF-74 (n/m)	[NO]=1000 ppm, [NH_3]=1000 ppm, [O_2]=2% If used: [H_2O] = no if used: [SO_2] = no Total flow= 100 ml/min	n/m	50,000	80	n/m	[49]
MIL-100(Fe-Mn) (n/m)	[NO]=500 ppm, [NH_3]=500 ppm, [O_2]=5% If used: [H_2O] = 5 vol.% if used: [SO_2] = 250 ppm Total flow= 100 ml/min	n/m	15,000	60	n/m	[14]
MOF-74-Mn (n/m)	[NO]=1000 ppm, [NH_3]=1000ppm, [O_2]=2% if used: [H_2O] = no if used: [SO_2] = no Total flow= 100 ml/min	60,000	n/m	45	n/m	[50]
Mn@CuBTC-0.05 (2.8 to 3.4 at.%)	[NO]=500 ppm, [NH_3]=500ppm, [O_2]=5% if used: [H_2O] = no if used: [SO_2] = no Total flow= 100 ml/min	n/m	30,000	70	n/m	[18]
Mn-MOF-74 (n/m)	[NO]= 500 ppm, [NH_3]=500 ppm, [O_2]=4% if used: [H_2O] = 5 vol.% if used: [SO_2] =no Total flow= 100 ml/min	n/m	50,000	75	n/m	[51]
MnOx/UiO-66-DP (assumed 8.5 wt.%)	[NO]= 500 ppm, [NH_3]=500 ppm, [O_2]=5% if used: [H_2O] = 5 vol.% if used: [SO_2] = 100 ppm Total flow= 100 ml/min	n/m	50,000	ca. 100	n/m	[52]
HKUST-1-Mn [a] (2.5 wt.%)	[NO]= 1000 ppm, [NH_3]=1000 ppm, [O_2]=8% if used: [H_2O] = 3.5 vol.% if used: [SO_2] =no Total flow= 100 ml/min	80,000	25,648	78 [b]	73 [b]	[27]
HKUST-1-Mn3.75 (3.74 wt.%)	[NO]= 1000 ppm, [NH_3]=1000 ppm, [O_2]=8% if used: [H_2O] = 3.5 vol.% if used: [SO_2] = 100 ppm Total flow= 167 ml/min	133,600	40,798	47	50	This study

n/m – not measured; [a] with assumed 2.5 wt.% of Mn loading [b] without presence of H_2O, when steady-state was obtained, i.e. after 510 min of NH_3-SCR experiment,

Entry for the Table of Contents

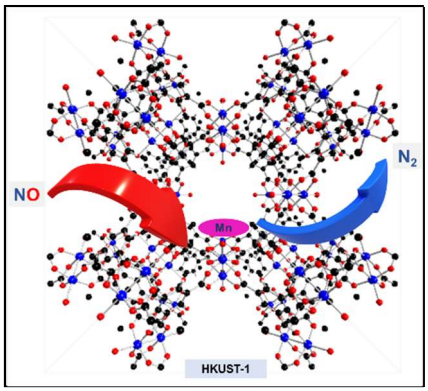

Selective catalytic reduction of NO by means of Mn impregnated HKUST-1 : The impregnation of Mn into HKUST-1 activates the catalytic reaction compared to the bare MOF. The conversion of NO reduction in presence of NH_3 at 185°C increases to ca. 70% with a manganese content up to 3.75 wt.%. The impregnation of manganese into HKUST-1 leads to structural and textural modifications evidenced by the creation of mesopores. The mesoporosity promotes the diffusion properties, allowing easy access of molecules to enhance the catalytic activity in the NH_3-SCR process.